LAWRENCE
LIVERMORE
NATIONAL
LABORATORY

UCRL-JRNL-200082

Computational Modeling of Vibration Damping in SMA Wires

P. Kloucek, D.R. Reynolds, T.I. Seidman

September 13, 2003

Continuum Mechanics and Thermodynamics

This document was prepared as an account of work sponsored by an agency of the United States Government. Neither the United States Government nor the University of California nor any of their employees, makes any warranty, express or implied, or assumes any legal liability or responsibility for the accuracy, completeness, or usefulness of any information, apparatus, product, or process disclosed, or represents that its use would not infringe privately owned rights. Reference herein to any specific commercial product, process, or service by trade name, trademark, manufacturer, or otherwise, does not necessarily constitute or imply its endorsement, recommendation, or favoring by the United States Government or the University of California. The views and opinions of authors expressed herein do not necessarily state or reflect those of the United States Government or the University of California, and shall not be used for advertising or product endorsement purposes.

This work was performed under the auspices of the U.S. Department of Energy by University of California, Lawrence Livermore National Laboratory under Contract W-7405-Eng-48.

Continuum Mechanics and Thermodynamics manuscript No.
(will be inserted by the editor)

Computational Modeling of Vibration Damping in SMA Wires

Petr Klouček[1], Daniel R. Reynolds[2], Thomas I. Seidman[3] ⋆

[1] Department of Computational and Applied Mathematics, Rice University, 6100 Main Street, Houston, TX 77005, USA
[2] Center for Applied Scientific Computing, Lawrence Livermore National Laboratory, P.O. Box 808, L-551, Livermore, CA 94551, USA
[3] Department of Mathematics and Statistics, University of Maryland Baltimore County, 1000 Hilltop Circle, Baltimore, MD, 21250, USA

Submitted May 16, 2003

Abstract. Through a mathematical and computational model of the physical behavior of shape memory alloy wires, this study shows that localized heating and cooling of such materials provides an effective means of damping vibrational energy. The thermally induced pseudo-elastic behavior of a shape memory wire is modeled using a continuum thermodynamic model and solved computationally as described by the authors in [23]. Computational experiments confirm that up to 80% of an initial shock of vibrational energy can be eliminated at the onset of a thermally-induced phase transformation through the use of spatially-distributed transformation regions along the length of a shape memory alloy wire.

Key words: thermodynamic control, active vibration damping, nonlinear partial differential equations, shape memory alloys
PACS: 02.60.Cb, 68.45.Kg, 64.70.Kb

1 Introduction

Shape memory alloys are characterized by their unique ability to undergo a thermally-induced crystal phase transformation, known as the first-order martensitic phase transformation. This transformation induces such materials to achieve up to 8% pseudo-elastic deformation (deformation without material damage) through small changes to their temperature. As a result of such uniquely sensitive responses to small temperature variations, these materials are currently being considered for such multi-ranging tasks as micro- and nano-machinery, biomedical implants, self-repairing shielding devices, and active damping applications.

⋆ The first two authors were supported in part by the grant NSF DMS–0107539, by the Los Alamos National Laboratory Computer Science Institute (LACSI) through LANL contract number 03891–99–23, as part of the prime contract W–7405–ENG-36 between the Department of Energy and the Regents of the University of California, by the grant NASA SECTP NAG5–8136, and by the grant from Schlumberger Foundation. The work of the second author was performed in part under the auspices of the U.S. Department of Energy by the University of California, Lawrence Livermore National Laboratory under Contract No. W–7405–Eng–48. All three authors were supported in part by a grant from the TRW Foundation. The computations in this paper were performed on a 16 processor SGI Origin 2000, which was partly funded by the NSF SCREMS grant DMS–9872009.

Correspondence to: P. Klouček (e-mail: kloucek@rice.edu), D. R. Reynolds (e-mail: reynoldd@llnl.gov), T. I. Seidman(e-mail: seidman@math.umbc.edu)

Our primary concerns in this paper are to test the applicability and feasibility of the computational approaches used for thermodynamic simulations, to gain insight into the internal mechanisms inducing vibrational damping, and to initiate exploration of control strategies for such damping in the shape memory alloy wires.

We use an improved thermodynamic model and solution method that correctly predicts all the relevant nonlinear behaviors inherent to shape memory alloy wires (see [23]). The model is used to examine the applicability of these materials for thermally-induced vibration damping. The computational experiments show that a promising thermal control for vibration damping purposes involves the formation of localized, regularly-spaced transformation regions along the length of the wire. Using such a controlling procedure, the thermally-induced crystal phase transformation achieves damping of up to 80% of the vibrational energy at the onset of the phase transition. The computational study of the damping mechanisms based on the SMAs, compatible with the widely used Likhatchev model [26], is reported by Oberaigner, Antretter, Fischer and Tanaka in [32].

We present the above topics in the following manner. Section 2 discusses the nonlinear thermodynamic model describing the thermodynamic behavior of these alloys, including both a new form of the inhomogeneous heat flux and a new construction of the free energy density. Then, Sections 3 and 4 describe the computational solution method used in solving the model, with special attention toward a new method for reducing errors introduced by artificial dissipation mechanisms. Finally, computational experiments showing the results on thermally-activated vibration damping are provided in Section 5. For the sake of completeness, in Section 7 we include some of the known theoretical results providing alternate mechanisms from the one used here for mechanical damping using shape memory alloys.

2 Mesoscopic Thermodynamic Model

The model is an expanded version of those discussed by Falk [10], Hoffmann and Songmu [16], Melnik and Roberts [28,29] and Niezgódka and Sprekels [31] in that we use a nonlinear, continuum physics based thermodynamic model of shape memory alloy wires, derived in [23,34]. This model improves upon the aforementioned models in a number of ways. First, the proposed model does not allow linear simplifications of the temperature response as in [8,10,22,21]. Such simplifications limit the applicability of those models to a small temperature region around the transition temperature and often decouple the resulting system of partial differential equations. Second, as opposed to the traditional Fourier heat flux, the model incorporates an inhomogeneous form of the heat flux that accounts for phase-dependent changes in the heat transfer, as proposed by R. D. James and P. Klouček [21] and Abeyaratne and Knowles [1]. A further improvement is that the model is based on a modified version of the Landau-Devonshire potential. The potential surmounts the difficulties of the Falk and Landau-Devonshire potentials, since it allows for control over the material constants for particular shape memory alloys, while still satisfying the theoretical requirements necessary for traditional existence theory. A final contribution of the model is that it solves the resulting nonlinear system of partial differential equations in a way that minimizes the artificial dissipation required by previous solution techniques. This section details the nonlinear thermodynamic model, which incorporates the inhomogeneous heat flux and improved free energy into the fully-coupled nonlinear model.

The spatial scale is the first consideration in constructing any model of material behavior. Compared to the time-scale of general thermodynamic processes, the first-order phase transformation itself occurs as a very sudden change on the molecular level ($\sim 10^{-9}$ m). However, molecular models encounter the major difficulty that computations must remain limited to a very small region, since each particle must be accounted for separately. Furthermore, on the molecular level such averaged quantities as temperature and entropy are not defined, and instead are replaced with particle kinetics. Macroscopic models ($\sim 10^{0}$ m) are similarly unhelpful, since the most interesting behaviors of these materials derive from the first-order phase transformation, which cannot be described by physical equations at the macroscopic level.

Therefore our model is on a scale between these two spatial levels. This *mesoscopic* scale ($\sim 10^{-5}$ m) consists of basic elements called *lattice particles*, which may be thought of as small parts of the continuum metallic lattice forming the body (see Huo, I. Müller and Seelecke [18]). Mesoscale models are based on the assumption that the usually negligible fluctuations of the molecular particles can be ignored (see Lifshitz and Pitaevskii [25]).

The choice of modeling on this mesoscopic scale has a number of consequences. First, at this scale the material can be thought of on a continuum level, where such thermodynamic quantities as the entropy and temperature are still defined. Moreover, mesoscale models assume that lattice particles transform between phases as whole units. In other words, at this level the microscopic crystal lattice deformations correspond to mesoscopic strains in the lattice particle. Therefore the mesoscopic strain may be considered as an order parameter. Thus, measurements of the mesoscopic strain permit recognition of individual material phases for each lattice particle (see Niezgódka and Sprekels [31]).

2.1 The Model

For our computational experiments on vibration damping using shape memory alloy wires, we use the nonlinear thermodynamic model derived by the authors in [23,34]. We begin by defining the quantities to be used throughout this paper in the following Table 2.1. The various material constants used are summarized in Table 2.2.

Variable	Units	Description
u	m	deformation
θ	K	absolute temperature
γ		deformation gradient, $\gamma = u_x$
b	N kg^{-1}	external body force
r	W kg^{-1}	external heat supply
q	W m^{-2}	referential heat flux
σ	Pa	first Piola-Kirchoff stress
η	J kg^{-1} K^{-1}	entropy density
ε	J kg^{-1}	internal energy density
Ψ	J kg^{-1}	Helmholtz free energy density

Table 2.1. Variables and their units used throughout the model. All quantities are defined for points (x, t) in the domain $\Omega \times I\!R^+$.

Remark 2.1 We make the following remarks on the variables and notation used throughout the thermodynamic model.

1. The reference configuration of the body is denoted $\Omega = [0, L] \subset I\!R$, which is shaped like a wire of length L having cross-sectional area β; reference lengths are here taken to be those of unstressed austenite in coordinatizing the wire.
2. Since we consider the deformation as opposed to the displacement, the austenitic reference configuration is therefore given by $u(x) = x$. One-dimensional deformation gradients $\gamma(x) \overset{\text{def}}{=} u_x(x) > 1$ thus imply local extension of the wire, and deformation gradients $\gamma(x) < 1$ imply local compression of the wire. The two martensitic deformation gradients are thereby given by $\gamma(x) = 1 \pm \gamma_0$, where γ_0 is a material property of the SMA.
3. The model is derived using a *Eulerian* frame of reference, i.e., we treat all quantities in regards to the reference configuration.
4. Due to the multiple, distinct stable phases of shape memory alloys, the deformation has limited regularity, $u \in L^2(I\!R^+; H^1(\Omega))$. Thus the deformation gradient $\gamma(x, t)$ is only defined *almost everywhere* $x \in \Omega$.
5. The Helmholtz free energy is defined according to Landau as $\Psi = \varepsilon - \theta\eta$, [25].
6. Derivatives, taken with respect to the reference frame, adhere to the following shorthand:
   - Time derivatives: $\frac{\partial}{\partial t} w(x, t) = \dot{w}(x, t)$;
   - Partial derivatives: $\frac{\partial}{\partial x} w(x, t) = \partial_x w(x, t)$ and $\frac{\partial^2}{\partial x \partial y} w(x, y) = \partial^2_{xy} w(x, y)$;
   - Total derivatives: $\frac{d}{dx} w(x) = \mathrm{d}w(x)$ and $\frac{d^2}{dx^2} w(x) = \mathrm{d}^2 w(x)$.

Constant	Units	Description
$1 \pm \gamma_0$		stable martensitic deformation gradients
ρ_0	kg m^{-3}	referential density
κ	W m^{-1} K^{-1}	thermal conductivity
c_p	J kg^{-1} K^{-1}	specific heat capacity
E_a	GPa	elastic modulus of austenite phase
E_m	GPa	elastic modulus of martensite phase
α	kg m^{-1} s^{-1}	viscosity coefficient
θ_A	K	austenite finish temperature
θ_C	K	critical transition temperature
θ_M	K	martensite finish temperature

Table 2.2. Material constants used in the model, along with their physical units.

7. Body forces are experienced as compressive vibrational stresses acting on the material elements at the $x = L$ end of the wire only; this end is also considered to be fully thermally insulated.
8. At the left end of the wire, $x = 0$, the temperature is fixed in a thermal bath at θ_{DC} and its deformation is held fixed at zero. The subscript DC indicates that we prescribe Dirichlet boundary condition at $x = 0$ for the temperature.
9. The body begins with initial deformation $u_0(x)$, initial velocity $v_0(x)$ and initial temperature distribution $\theta_0(x)$.
10. We assume that the referential density is homogeneous throughout the body. □

The thermodynamic model considers the fully-coupled nonlinear system of equations given by the balance of linear momentum and the conservation of energy to describe the thermodynamic behavior of a broad class of materials. Often, the solutions to these equations are considered separately, where one alternates between solving one equation and then the other. However, those approaches may be flawed due to the sudden changes in the thermodynamic state at moments of phase transition. In view of the dependence of both equations on the thermodynamic quantities u and θ, such operator-splitting techniques may not be applicable. Therefore, we instead consider the fully coupled, nonlinear system of partial differential equations given by

$$\begin{aligned} \rho_0 \ddot{u} &= \rho_0 \partial^2_{x\gamma} \Psi + \alpha\, \partial^2_{xx} \dot{u} + \rho_0 b \\ \rho_0 c_p \dot{\theta} &= \rho_0 \theta \partial^2_{\gamma\theta} \Psi \dot{\gamma} + \alpha\, \dot{\gamma}^2 + \kappa \partial_x \left(\gamma \partial_x \theta \right) + \rho_0 r; \end{aligned} \tag{2.1}$$

with the experimental conditions dictating the initial and boundary conditions

$$\begin{aligned} &u(x,t_0) = u_0, \quad \dot{u}(x,t_0) = v_0, \quad \theta(x,t_0) = \theta_0 \\ &u(0,t) = 0, \quad \dot{u}(0,t) = 0, \quad \theta(0,t) = \theta_{\mathrm{DC}}(t), \quad \partial_x \theta(L,t) = 0. \end{aligned}$$

We note that the current model ignores possible heat dissipation to the environment. Furthermore, the behavior of the SMA wire is controlled through the heat supply term $r(x,t)$. The vibrational forces are implemented in the body force term $b(x,t)$, and affect the material at the $x = L$ end of the wire. These forces are implemented as a force acting on the material elements in a small amount of the material in the spatial interval $(L - \delta x, L)$.

At the heart of this model is the Helmholtz free energy $\Psi(\gamma,\theta)$. We use the following form, derived in [23,34],

$$\Psi(\gamma,\theta) = C_M(\theta)\mathcal{W}_M(\gamma) + C_C(\theta)\mathcal{W}_C(\gamma) + C_A(\theta)\mathcal{W}_A(\gamma) + c_p(\theta - \theta\ln\theta) + D\theta + E,$$

where

$$\begin{aligned}
\mathcal{W}_M(\gamma) &= \begin{cases} \frac{E_m}{2\rho_0}(\gamma-1-\gamma_0)^2, & \gamma < 1-\gamma_0, \\ \frac{E_m}{8\rho_0\gamma_0^2}\left((\gamma-1)^4 - 2\gamma_0^2(\gamma-1)^2 + \gamma_0^4\right), & \gamma \in [1-\gamma_0, 1+\gamma_0], \\ \frac{E_m}{2\rho_0}(\gamma-1+\gamma_0)^2, & \gamma > 1+\gamma_0; \end{cases} \\
\mathcal{W}_C(\gamma) &= \begin{cases} \frac{E_a+E_m}{4\rho_0}(\gamma-1-\gamma_0)^2, & \gamma < 1-\gamma_0, \\ \frac{E_a+E_m}{16\rho_0\gamma_0^4}\left((\gamma-1)^6 - 2\gamma_0^2(\gamma-1)^4 + \gamma_0^4(\gamma-1)^2\right), & \gamma \in [1-\gamma_0, 1+\gamma_0], \\ \frac{E_a+E_m}{4\rho_0}(\gamma-1+\gamma_0)^2, & \gamma > 1+\gamma_0; \end{cases} \\
\mathcal{W}_A(\gamma) &= \frac{E_a}{2\rho_0}(\gamma-1)^2;
\end{aligned} \tag{2.2}$$

the various constants are defined in Table 2.2; and the coefficient functions $C_M(\theta)$, $C_C(\theta)$ and $C_A(\theta)$ are constructed to piece the isotherms $\mathcal{W}_M$, $\mathcal{W}_C$ and $\mathcal{W}_A$ together using natural cubic splines on a regular temperature mesh containing the set of temperatures $\{\theta_M, \theta_C, \theta_A\}$. Thus we omit the formulae for these coefficients. The system (2.1) is solved to find the thermodynamic state (u and θ) in the shape memory alloy wire at any point $(x,t) \in [0,L] \times [0,\infty)$.

By construction, the free energy Ψ satisfies the requirements dictated by the physical behavior of shape memory alloy wires. The free energy accounts for the phenomenological behavior of shape memory alloys through the first-order phase transformation. Moreover, not only is the form (2.2) for the free energy qualitatively correct, but it is rich enough to allow enough control over the material behavior for good approximation of particular SMAs. Therefore the general thermodynamic model (2.1), with the Helmholtz free energy (2.2) at its core, fully describes the nonlinear thermodynamic behavior of shape memory alloys.

Before presenting our computational results using the proposed model, however, we discuss the methods used for approximating weak solutions to the system (2.1). Given the existence theory for such systems by Friesecke and Dolzmann [14] and Niezgódka and Sprekels [31], we discuss the proposed computational solution method in the following Sections 3 and 4.

3 Continuous Space-Time Galerkin

We now consider the computational solution of the proposed model. Of particular importance in the numerical solution of such hyperbolic systems of conservation laws is the necessity for the discrete scheme to satisfy discrete versions of those conservation laws. This means that the discrete scheme used to compute solutions to the continuous Lyapunov system (2.1) must in turn provide a discrete Lyapunov system. This discrete analog of conservation of energy assures the long-time stability of the approximate solution and provides a discrete total thermomechanical energy which will remain unconditionally conservative or even dissipative in time.

For this purpose we employ *Continuous Time Galerkin* (CTG) Methods for the time-discretization of our PDE system. CTG methods were first introduced in the context of ordinary differential equations by Hulme [17], and further expanded by French and Jensen [12] and French and Peterson [13]. According to these studies, CTG methods satisfy the required Lyapunov stability in time. This occurs because such methods retain continuity in time, so discrete versions of the energy conservation principles remain applicable to the resulting discrete systems. It is known that other numerical methods, such as the method of lines and various integral methods, also satisfy this discrete Lyapunov property. However, the further benefit to CTG schemes is that, when combined with finite element approximations of the spatial variables, they provide for a unified treatment of both spatial and temporal discretization. Furthermore, CTG methods allow for a systematic method of proving existence of discrete solutions for long time scales, through examination of the Lyapunov nature of the total energy in time. Continuous Time Galerkin methods have thus been used successfully in the approximation of solutions to nonlinear wave equations similar to that used in the current model (see [13,15,20–22] for further details).

4 Variable Viscosity Newton Method

Due to the non-convexity of the free energy (2.2), time and space discretization of the PDE system (2.1) results in a finite-dimensional, nonlinear, nonconvex root-finding problem. In this resulting problem, local minima of the root-finding surface correspond to unphysical thermodynamic states, and therefore a more global optimization method is desired. Since traditional optimization methods prove insufficient in this case, we return to the existing literature on the problem of phase transitions. From considering the success of methods on the perturbed problems having high viscosity coefficients (see Friesecke and Dolzmann [14], Hoffmann and Songmu [16] and Niezgódka and Sprekels [31]), and due to the similarity to the well-known Method of Vanishing Viscosity used in the solution of scalar conservation laws (see Dafermos [7] or Málek, Nečas, Rokyta and Růžička [27]), we propose the following *variable viscosity approach* for the model solution. In this approach the moment of phase transition is detected by monitoring iterates in the damped Newton method. Once these iterates show signs of stagnation, and thus phase transition in the model solution, the viscosity coefficient α is increased to the level proposed by theoretical results in order to render the model well-posed. The standard Newton method is then applied to this perturbed system to obtain a perturbed solution for the current time step. From this point, the viscosity level α is progressively lowered, using the previous perturbed solutions as the initial guesses for the Newton root-finding scheme to better calculate the same time step. Denoting the original zero-viscosity root-finding problem as $\tilde{\mathbf{g}}(X,\varphi) = \mathbf{g}^{n,\Delta x}(X^{n-1}, X^n, \varphi) = 0$ with corresponding solution X^*, and denoting the viscosity-perturbed problem as $\tilde{\mathbf{g}}^{\alpha}(X,\varphi) = 0$ with corresponding solution X^{α}, this process may be written in the following manner:

Definition 4.1 (Variable Viscosity Newton Method)

0. *Initialize* $\alpha = 0$ *and* $X = X^n$.
1. *Construct the linear system* $D\tilde{\mathbf{g}}(X,\varphi)(\overline{X}) = -\tilde{\mathbf{g}}(X,\varphi)$, *where*

$$D\tilde{\mathbf{g}}(X,\varphi)(\overline{X}) = \begin{bmatrix} D\tilde{g}_1(X,\varphi)(\overline{u}) & D\tilde{g}_1(X,\varphi)(\overline{v}) & 0 \\ D\tilde{g}_2(X,\varphi)(\overline{u}) & D\tilde{g}_2(X,\varphi)(\overline{v}) & D\tilde{g}_2(X,\varphi)(\overline{\theta}) \\ D\tilde{g}_3(X,\varphi_k)(\overline{u}) & 0 & D\tilde{g}_3(X,\varphi)(\overline{\theta}) \end{bmatrix}$$

$$\overline{X} = \begin{bmatrix} \overline{u} & \overline{v} & \overline{\theta} \end{bmatrix}^T$$

$$\tilde{\mathbf{g}}(X,\varphi) = \left[\tilde{g}_1(X,\varphi) \quad \tilde{g}_2(X,\varphi) \quad \tilde{g}_3(X,\varphi)\right]^T.$$

2. *Attempt to solve the above system for* $\overline{X}$. *If no solution exists, then the system is stuck at a local minimum. Skip to step 5.*
3. *Set* $\tau = 1$ *and halve* τ *progressively until* $\tilde{\mathbf{g}}(X + \tau\overline{X},\varphi) < \tilde{\mathbf{g}}(X,\varphi)$. *If this fails, or if* τ *decreases below a minimum tolerance, then the system is approaching a local minimum. Skip to step 5.*
4. *Update the Newton iterate* $X = X + \tau\overline{X}$. *If the stopping criteria is met, exit. Otherwise return to step 1.*
5. *Set* $\alpha = \alpha_{max}$ *and* $X^{\alpha} = X^n$.
6. *Construct the linear system*

$$D\tilde{\mathbf{g}}^{\alpha}(X^{\alpha},\varphi)(\overline{X}) = -\tilde{\mathbf{g}}^{\alpha}(X^{\alpha},\varphi).$$

7. *Attempt to solve the above system for* $\overline{X}$. *If no solution exists, return* X^{α} *as the final perturbed solution.*
8. *Update the viscous Newton iterate* $X^{\alpha} = X^{\alpha} + \overline{X}$. *If the Newton stopping criteria is met, halve* α. *Return to step 6.*

The above algorithm is designed to serve two key purposes. First, it assures that the overall time-stepping scheme remains stable by reverting to the solution of the perturbed, parabolic system $\tilde{\mathbf{g}}^{\alpha}(X,\varphi)$

during moments of computational difficulty. Second, the viscous Newton method shown here reduces the amount of error in the solution to the dynamic system introduced through the artificial dissipation. Typically, the method as described here achieves solutions to perturbed systems using viscosity coefficients at least an order of magnitude smaller than those required without reduction of the viscosity (see [14,33]).

Viscous stresses are included in the model using the term $\alpha\dot{\gamma}$. The use of such additional viscous stresses has no physical justification, since any internal conversion of mechanical to thermal energy should be accounted for through the nonlinearity of the model [3–5,14,35,30]. Therefore, the true physical case of a SMA wire corresponds to viscosity coefficient $\alpha = 0$. Rather, these additional viscous stresses are included in the model to avoid possible ill-posedness at the onset and during the phase transition. The ill-posedness is caused by the construction of the Helmholtz free energy which connects the equilibria by the thermodynamic states at which the energy can be negative definite. Such states are considered unphysical, [9].

In essence, the variable viscosity method proposed here provides a practical trade-off between modeling accuracy ($\alpha = 0$) which may result in unphysical fluctuations, and computability ($\alpha > 0$) which results in artificial smoothing of the computed function. The proposed method achieves this through updating the viscosity coefficient to move from the large viscosity solution to the small viscosity solution.

5 Computational Experiments

We have examined in [24] the theoretical possibilities of using temperature as an active control to damp vibrational energy in SMA wires. Our theoretical results show that damping may be possible through the use of oscillatory temperature controls. The computational results in the following sections are designed to investigate various means of implementing such a strategy to damp vibrations in shape memory alloy wires. To this end, we present results on how the temperature-induced full phase transformation and spatially-localized phase transformations affect vibrational energy in a shape memory alloy wire[1]. We conclude the computational results by discussing a highly effective temperature control for these damping processes.

Constant	Value	Units	Description
γ_0	0.02		stable martensitic displacement gradient
ρ_0	6.45×10^3	kg m^{-3}	density
κ	10	W m^{-1} K^{-1}	thermal conductivity
c_p	322	J kg^{-1} K^{-1}	specific heat capacity
E_a	7.5×10^{10}	Pa	austenite elastic modulus
E_m	2.8×10^{10}	Pa	martensite elastic modulus
$1 \pm \gamma_0$	1 ± 0.02		stable martensitic strains
L	0.05	m	length of wire
β	2×10^{-8}	m^2	cross-sectional area of wire
θ_A	350	K	austenite finish temperature
θ_C	335	K	critical transition temperature
θ_M	320	K	martensite finish temperature

Table 5.1. NiTi material constants used within the calculations (from [6,19]).

In all these numerical experiments, we consider the NiTi shape memory alloy (though given the correct set of material constants, other alloys could be tested as well). The material constants used throughout the numerical experiments are given in Table 5. However, before presenting results from the numerical simulations, we discuss some of the visualization techniques used to represent output from the one-dimensional thermodynamic model.

---

[1] The model's ability to perform the stress-induced phase transformation is demonstrated in [23].

5.1 Visualization Techniques

In order for the computational results in the remainder of the section to be easily interpreted, we discuss some of the methods used to visually represent the numerical results. The greatest difficulty in showing the computational results lies in finding meaningful representations of the deformation and material phases through the shape memory alloy wire. One-dimensional deformations constitute elongation ($u_x(x) > 1$) and contraction ($u_x(x) < 1$). But since macroscopic length changes are difficult to observe and do not provide information as to local changes in the wire, we plot the *displacement*, instead of the deformation. Thus, plots of the physical shape changes in the wire will show, on the vertical axis, distances away from the austenitic reference configuration. Therefore, positive values of displacement correspond to elongation and negative values to contraction, as seen in Figure 5.1. With this visualization technique, austenitic regions seem "flatter" in these plots than martensitic regions, which have steeper displacement gradients. Furthermore, as a result of the steeper displacement gradients, twinned martensite appears highly oscillatory, as seen on the right side of the example displacement plot in Figure 5.1.

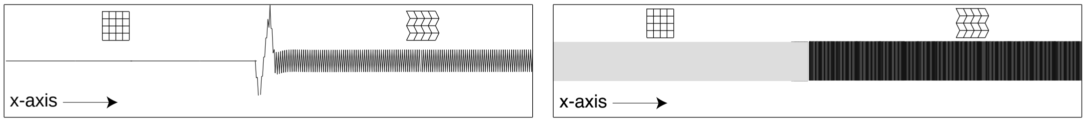

Fig. 5.1. Displacement and Phase Visualization Techniques: One dimensional deformation constitutes elongation and contraction. Thus displacement (left plot) is plotted for clarity, with positive values corresponding to elongation and negative values corresponding to contraction. Phase plots (right side) use *light gray* as the austenite phase, and use *medium gray* and *dark gray* for the martensite variants. Note the austenitic regions in the left side of both plots, and the martensitic regions in the right side of each plot.

We must also plot meaningful results for the various material phases at different locations along the wire. Since the material phases at equilibrium correspond to $\gamma(x) = 1$ for austenite and $\gamma(x) = 1 \pm \gamma_0$ for martensite, and also since these dynamic experiments allow for deviations away from equilibrium, we may simply choose between the phases in the following manner: at each point x in the wire,

$$\begin{array}{rcl} \gamma(x) \geq 1 + \gamma_0/2 & \Rightarrow & \text{martensite}^+, \\ \gamma(x) \leq 1 - \gamma_0/2 & \Rightarrow & \text{martensite}^-, \\ |\gamma(x) - 1| < \gamma_0/2 & \Rightarrow & \text{austenite}. \end{array}$$

We then use grayscale plots to show these phases, along with the corresponding length change in the wire, as shown in Figure 5.1, where *light gray* regions correspond to austenite, *medium gray* regions to martensite$^+$ and *dark gray* regions to martensite$^-$. The twinned martensite is shown by the rapid alternation between each of the detwinned states as seen in Figure 5.1.

Other plots that are used to represent the numerical results are the kinetic energy and the temperature. The temperature plots are straightforward, however the kinetic energy plots are slightly more complex. An example plot showing the time-evolution of the overall kinetic energy (in Joules) in the wire, as calculated via

$$\mathcal{K}(t) = \rho_0 \beta \int_0^L v(x,t)^2 \mathrm{d}x, \tag{5.1}$$

may be seen in Figure 5.2. Here, the highly oscillatory behavior in time is a result of the exchange between potential and kinetic energy in the wire. To obtain an idea of the time-behavior of the overall vibrational energy in the wire, it suffices to follow the peaks of this curve in time.

With these visualization tools at our disposal, we now demonstrate the vibration damping experiments using simulated shape memory alloy wires. We begin with the general experimental setup.

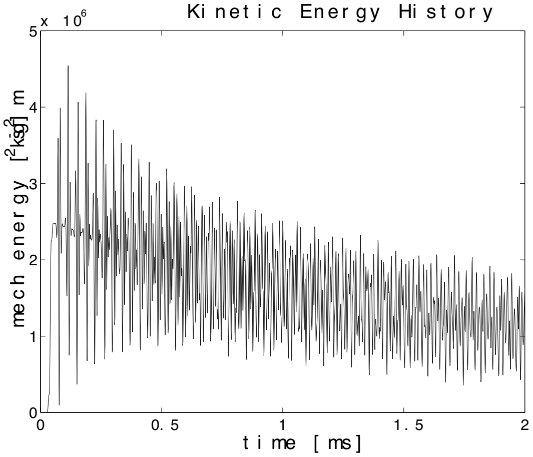

Fig. 5.2. Kinetic Energy Visualization Technique: Kinetic energy plots oscillate rapidly as a result of the exchange between kinetic and potential energy. The overall vibrational energy may be tracked by following the peaks.

5.2 Damping Strategy

These examples are designed to elucidate the applicability of the NiTi shape memory alloy for vibration damping purposes. Each of these examples begins with the wire at rest. Early into the simulations, a vibrational wave of the form

$$b((L - \Delta x, L), t) = \mathbf{mag} * \cos\left(\frac{t - \mathbf{peak}}{\mathbf{dur}}\right) * \exp\left(-\left(\frac{t - \mathbf{peak}}{\mathbf{dur}}\right)^2\right)$$

strikes the free end of the wire, where **mag** provides the magnitude of the wave, **peak** provides the time of the wave peak, and **dur** provides the duration of the vibrational activity. The values of these parameters used in the following experiments were **mag** $= 2 * 10^4$ N kg^{-1}, **dur** $= 0.04$ ms and **peak** $= 0.04$ ms. A picture of the resulting vibrational wave is given in Figure 5.3. This form of vibrational energy is used since it allows for a short but strong burst of vibrational energy to enter the wire, and from that moment we may analyze the damping behavior in time. We implement the vibrational forces as a body force, acting only within the rightmost end of the wire. This allows us to include external forces without need of surface forces on the boundary.

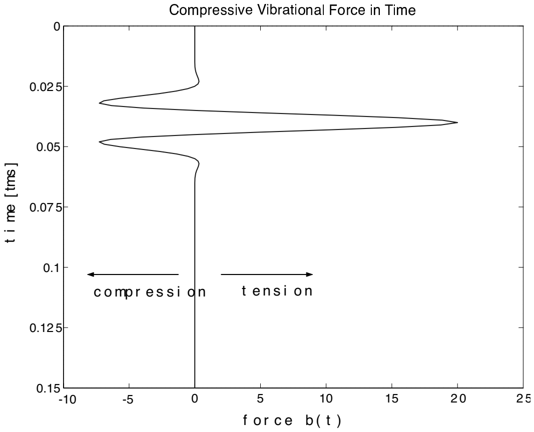

Fig. 5.3. Vibrational Force Used in Damping Tests: the tensile/compressive body force $b(t)$ exerted on the rightmost end of the wire, and measured in units kN kg^{-1}. The axes are swapped, with time proceeding downward, to indicate the direction of force. Note the truncated time scale, since the full simulation lasts 2 ms.

Each of the following four examples begins with the wire in the fully-twinned martensitic state at the transition temperature θ_C, and the same vibrational wave affects each of them at the beginning of the simulation. After the initial wave hits, the examples differ in only the heating and cooling schemes used to combat the vibrational waves. The first of these examples in Section 5.3 provides the base case in the absence of any temperature control. This serves as the point of comparison for the subsequent examples. The second example, in Section 5.4, shows the effects of a full phase transformation on the vibrational energy in the wire. The third example, discussed in Section 5.5, shows how highly localized phase transformations perform for damping applications. The final example, in Section 5.6, shows a promising means for using localized phase transformations to damp vibrational energy. A more complete set of numerical experiments including annotations and analyses of robustness and numerical stability can be found at *http://www.caam.rice.edu/∼reynoldd/*.

5.3 Base Case

This example is used as a base of comparison for the various heating schemes. Therefore no heating control is applied to the wire, and the results provide the comparative case of a purely vibrating martensitic wire.

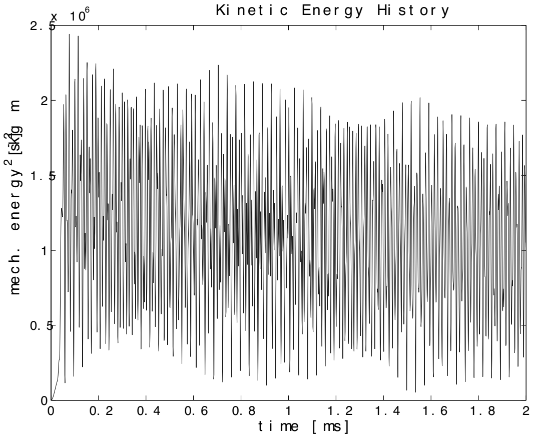

Fig. 5.4. Kinetic Energy Plot for an Uncontrolled Vibrating Wire: Note the very slow natural damping.

The Figure 5.4 shows the kinetic energy history for the uncontrolled case. As expected, the vibrational energy very slowly damps out of the system. The apparent random nature of the vibrational waves is likely due to the frequencies of the input wave being out of synchrony with the natural frequencies in the wire. It is expected that as time goes on, the higher frequency vibrations will slowly cancel out, while the lower frequencies will remain, steadily vibrating the shape memory wire in time.

The temperature and phase plots of this case are of little interest, since the temperature remains within 0.01 K of the initial temperature θ_C and neither the temperatures nor stresses are large enough to create the austenitic phase in the wire. Thus we limit the snapshot plots for this example to those of the displacements in Figure 5.5, taken at the equidistant time levels $t = 0.1$ ms, 0.7 ms, 1.3 ms and 1.9 ms. As expected, the plots show the motion of the vibrational waves through the martensitic wire in time.

Certainly, this case is of little interest in its own right. However, the remaining examples, when compared with both the kinetic energy plot and the displacement plots here, provide both unexpected and interesting results.

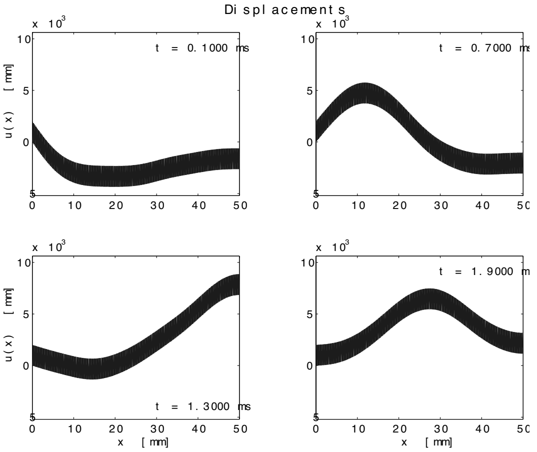

Fig. 5.5. Displacement Plots for the Uncontrolled Vibrating Wire: The martensitic wire vibrates under wave motion. Temperatures and stresses are too small to induce transformation.

5.4 Non-Localized Phase Transformation

In this first of our examples of thermal control for the damping of vibrations in shape memory alloy wires, we examine the effect of transforming the entire wire from martensite to austenite. To this end, we uniformly heat the wire throughout the simulation using the control $r(x,t) = 6$ kJ g^{-1} ms^{-1}. The amount of the heat pumped into the wire is large hence the relaxation times are short. We use this as a calibration of the model since we can thus allow for short time span for our experiments. However, the increased amount of added heat does not change the qualitative conclusions on damping vibrational energy. The thermally-induced phase transformation occurs in two stages. In this example, the first of these occurs at $t = 0.8$ ms. Then, due to the effects of latent heat, the second stage of the phase transformation occurs at $t = 1.1$ ms. The behavior of the kinetic energy just before, during, and after these partial phase transformations proves to be quite interesting. As seen in the time history of the kinetic energy in Figure 5.6, as the temperature increases the kinetic energy slowly decreases. Then, at the onset of the first stage in the phase transformation, the kinetic energy drops suddenly. When this first stage of the phase transformation is complete, there is a brief spike in the kinetic energy before the second stage of transformation begins. However, when this second stage is complete, the overall kinetic energy in the wire is significantly larger than when the simulation began.

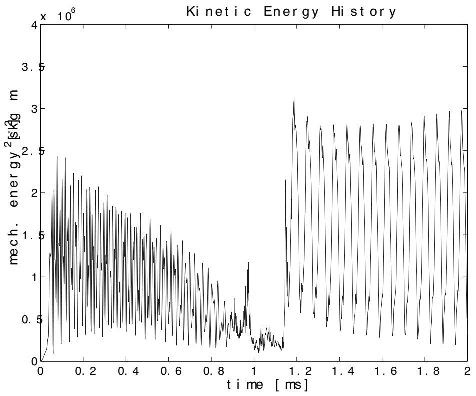

Fig. 5.6. Kinetic Energy Plot for the Non-Localized Phase Transformation: The kinetic energy decreases as the wire is heated. At the moment of phase transformation kinetic energy drops significantly, followed by energy spikes. Note the final highly regular, larger observable vibrational energy.

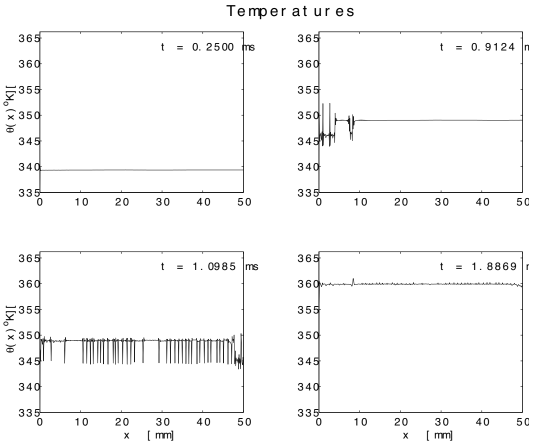

Fig. 5.7. Temperature Plots for the Non-Localized Phase Transformation: The temperature-induced phase transformation proceeds as normal, though begins at the leftmost end of the wire.

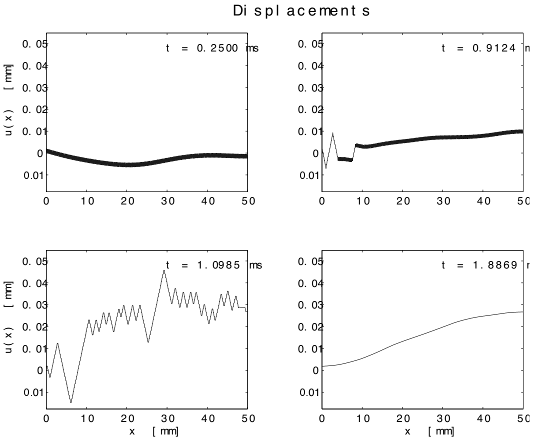

Fig. 5.8. Displacement Plots for the Non-Localized Phase Transformation: the vibrating wire undergoes the two-stage phase transformation. Note that the transformation begins at the fixed end of the wire, due to increased stress at that end.

We believe that all of these processes may be explained simultaneously as conversion between various kinds of energy. After the initial wave hits the wire, vibrations oscillate rapidly in a seemingly random fashion, with significant amounts in both the kinetic and potential energy states. Then, as the temperature is increased, the energetic metastability of the martensitic phase increases. The increase in metastability corresponds with a conversion of a significant amount of the kinetic energy to potential energy in the wire. As the phase transition itself occurs, the potential energy reaches its peak, causing a brief calm in the wire before the first transformation suddenly "pops" a significant amount of the wire into the austenitic state, increasing the kinetic energy dramatically. However, since the second stage of the phase transition is beginning, the kinetic energy is once again converted into potential energy. Finally, when the full phase transformation is complete, the potential energy is released. When this occurs, the resulting vibrations resonate at one of the wire's natural frequencies, causing the larger peaks and more regular structure of the kinetic energy.

Plots of the temperature distribution, displacements and phases at the time levels $t = 0.25$ ms, 0.9124 ms, 1.0985 ms and 1.8869 ms are shown in Figures 5.7, 5.8 and 5.9, respectively. As seen in these plots, the thermally-induced phase transformation occurs similarly as before, occurring first through about half of the wire and then continuing through the rest in the second stage of the transformation.

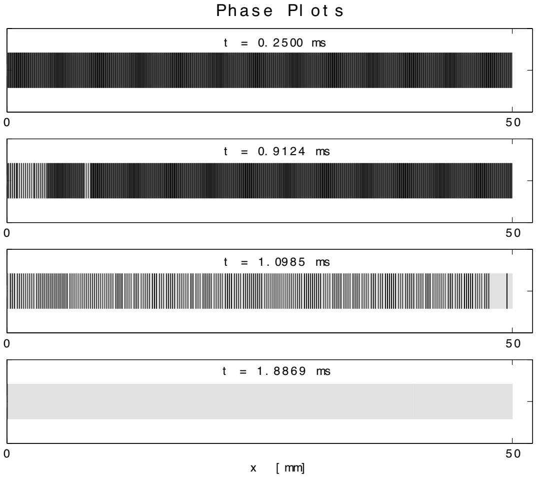

Fig. 5.9. Phase Plots for the Full Transformation: The phase transformation occurs throughout the entire length of the wire in a distributional nature in two stages.

It is notable, though, that unlike the static case, the transformation begins in the vibrating wire at the fixed (left) end of the wire. We believe that this is due to the increased amount of stress experienced when waves reflect off of this end. When these reflections occur, the stress at the fixed end becomes maximal before sending the wave energy back through the wire. Thus at the moment of reflection, the increased stress level provides an initial starting point for the phase transformation to begin. Then as a result of the increase in the overall temperature distribution, the remainder of the wire transforms soon after.

5.5 Localized Phase Transformations

Since the non-localized phase transformation resulted in an *increase* in the observable kinetic energy of the wire, a natural reaction is to test the effect of localized phase transformations as a control mechanism. In this example, we examine the affect of transforming highly localized areas of the wire from martensite to austenite. To this end, we unevenly heat the wire using the control

$$r(x,t) = 10\,\sin\left(2\pi * (x + t/2)\right) \;\; \text{kJ g}^{-1}\;\text{ms}^{-1}.$$

This heating control allows for both a localization of the heat control, as well as a motion of the heat in time. Due to the form of the control, there are a large number of full sine waves periodically heating and cooling the wire. Furthermore, due to the relatively large factor of 2 dividing the time (the total time $T = 2$ ms), the heating control moves slowly along the length of the wire as the simulation proceeds, allowing the temperature of the highly-localized regions to reach the required transformation temperatures. Lastly, although this three-parameter (amplitude, localization and speed) form of the heat supply amounts to a very simple form of the thermal control, it serves as an illustrative example for understanding how localization of the heat control benefits the vibrational damping.

Figure 5.10 provides the kinetic energy history of this experiment. In this plot we see that, as in the example of the full phase transformation, the kinetic energy again decreases slowly as the temperature is increased through local regions in the wire. Moreover, when the phase transformation begins in the wire at the time $t = 0.5$ ms, the kinetic energy drops suddenly. When this distributed phase transformation is complete, the kinetic energy again increases; however, the subsequent transformations cancel out most of the kinetic energy from the system.

These results may be analyzed in relation to the locality of the phase transformations. As seen in the previous example, the sudden phase transformation resulted in an abrupt burst of kinetic energy that then resonated at the characteristic speed of the austenitic phase in the wire. Similarly, the localized phase transformations of the current example induce bursts of vibrational energy. However,

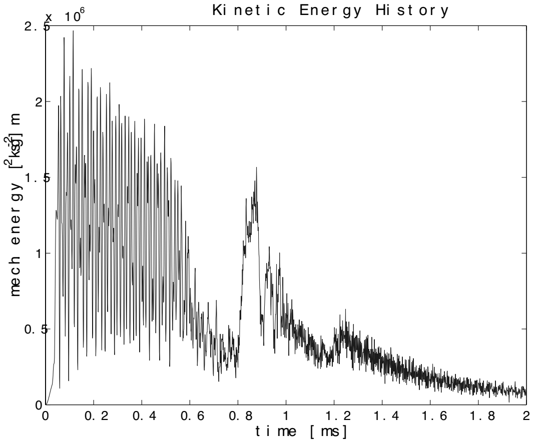

Fig. 5.10. Kinetic Energy Plot for the Highly-Localized Phase Transformation: The highly-localized phase transformation results in cancellation of the induced vibrational waves following an initial spike in the kinetic energy.

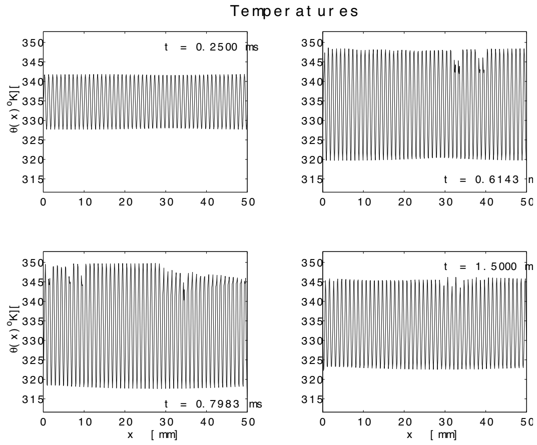

Fig. 5.11. Temperature Plots for the Highly-Localized Phase Transformation: The thermal control results in oscillatory temperatures through the wire. Latent heat effects decrease the peaks in transforming regions.

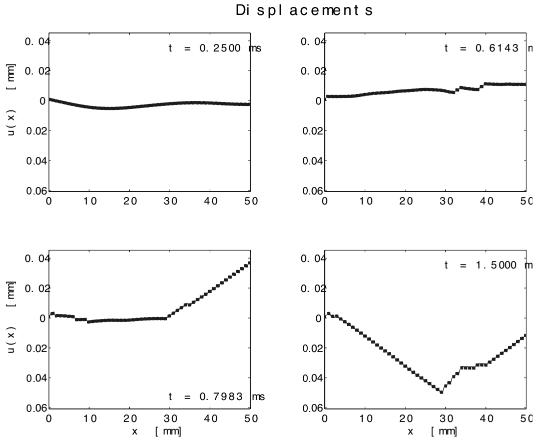

Fig. 5.12. Displacement Plots for the Highly-Localized Phase Transformation: A large number of very small regions transform states; however, these small regions significantly affect displacements along the wire.

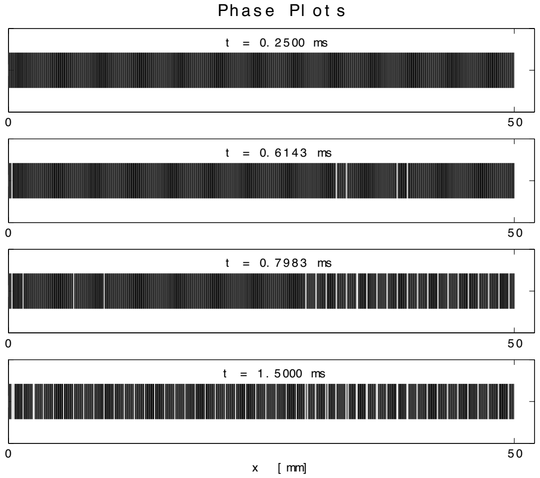

Fig. 5.13. Phase Plots for the Highly-Localized Transformation: The small, transformed regions along the wire are seen as the appearance of thin light gray lines among the predominantly martensitic state of the wire.

in this case the distributed nature of the phase transformation regions leaves regularly-spaced regions in which these vibrations travel. Since the induced vibrations travel at the same speeds through these untransformed regions, the self-cancellation of such anti-phase vibrations results in the overall damping observed in the experiment.

The effect of the slow-moving, highly-localized heat control r on the temperature distribution may be seen in Figure 5.11. As time progresses, the temperatures in these small regions grow due to the slow motion of the control. In the second and third plots, the effects of latent heat from the localized transformation can be observed. Finally, we note that due to the movement of the heating control, the temperature waves begin shrinking again as the control moves away from its initial position.

As seen in Figure 5.12, the displacement plots also show the effect of localized phase transformations on the shape memory wire. Although these transformations only occur on a relatively small amount of the overall length, they have a significant effect on the resulting displacements in the wire. Finally, Figure 5.13 shows the phase distributions along the shape memory wire in time. Here, the regularly-spaced regions of light gray in the lower plots show the locations of the phase transformations.

5.6 "Best Case" Damping Scheme

The best results on vibration damping that we have yet found result from a less localized thermal control than in the previous example. In this experiment, we again use a localized, slow-moving temperature control having the same overall magnitude; however, in this case the localization is more coarse than before. The temperature control r is given in this example by

$$r(x,t) = 10\,\sin\left(2\pi * (x/10 + t/2)\right)\ \ \mathrm{kJ\ g^{-1}\ ms^{-1}},$$

which results in only five complete thermal waves, as opposed to the fifty in the previous example. The resulting kinetic energy history is given in Figure 5.14. The general behavior of the vibrational energy is nearly identical to that of the example 5.5, though the temperature spike after the initial transformation no longer appears. We believe this is a result of the larger transformation regions, along with the larger distance the induced vibrations travel before encountering each other and canceling.

The resulting time level plots of the temperature are given in Figure 5.15. As seen in these plots, when the peaks of the thermal control reach the austenitic transformation temperature those spatial control regions transform. These transformation again cause a release of latent heat, having a pronounced effect on the resulting temperature distribution. Furthermore, as this thermal control moves to the right, the temperature variations begin to diminish.

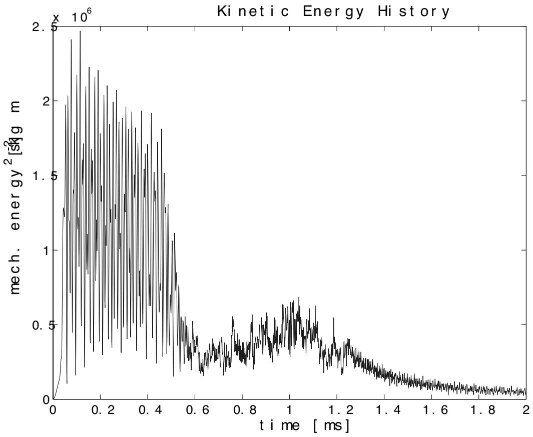

Fig. 5.14. Kinetic Energy Plot for the "Best Case" Temperature Control: Again, the onset of the phase transformation damps the wire, though this time the larger phase transformation regions do not result in a spike of kinetic energy.

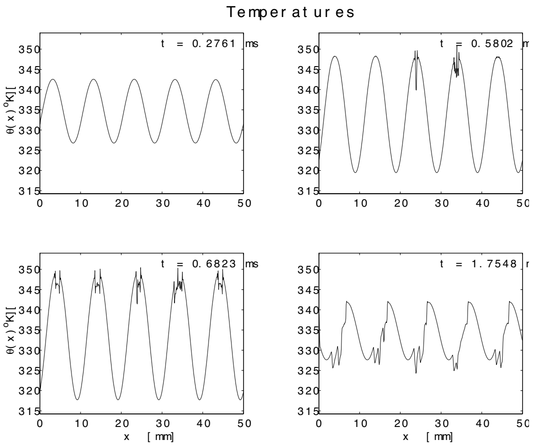

Fig. 5.15. Temperature Plots for the "Best Case" Temperature Control: the heating control results in smoother temperature distributions, with larger transformation regions. Note that the slow movement of the thermal control in time brings the temperatures back toward the transformation temperature $\theta_C = 335$ K.

The resulting transformation regions can also be clearly seen in the displacement plots of Figure 5.16. As seen here, very few of the localized transformation regions exist as purely austenite; instead these regions have mostly undergone only one stage of the thermal transformation, leaving regularly-spaced mixtures of austenitic and martensitic variants. We believe that the regular spacing of these transformations is of vital importance to the large degree of damping that results, as evidenced by Figure 5.14.

Finally, the phase plots of Figure 5.17 show two important characteristics of these localized damping regions. First, as seen by tracking the end of the wire, the macroscopic length of the simulated wire remains virtually unchanged, even though the phase transformations within the wire have changed the local structure. Also, this figure clearly shows the slow movement of the transformation regions to the right (toward $x = L$), as seen from the difference between the timelevel states $t = 0.6823$ ms and $t = 1.7548$ ms.

5.7 Variable Viscosity Effects on Damping

We conclude with computational results showing that the damping results from Section 5.6 do not arise from the increased viscosities at the onset of the thermally-induced phase transformation resulting from

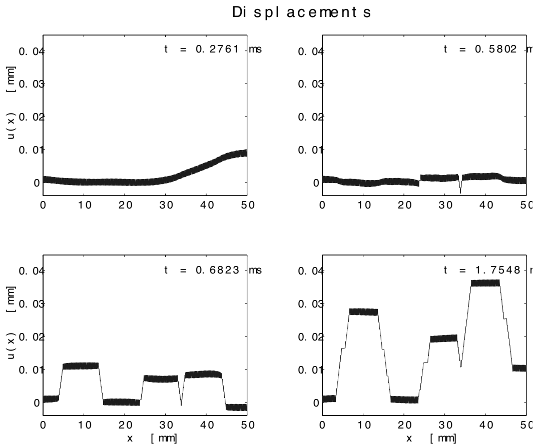

Fig. 5.16. Displacement Plots for the "Best Case" Temperature Control: Here there are larger transformation regions, as well as longer areas of untransformed martensite. We believe these two factors play a key role in the additional damping ability resulting from this heating scheme.

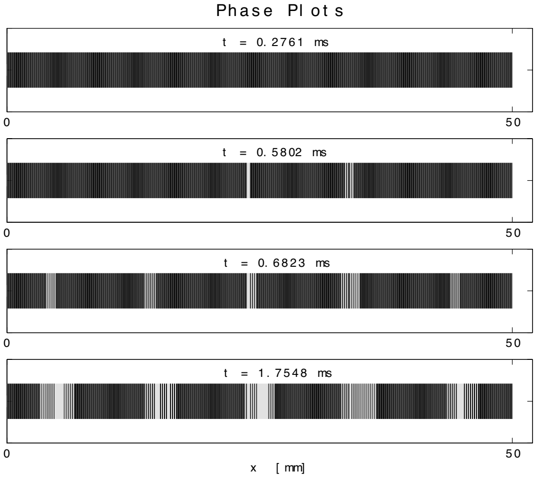

Fig. 5.17. Phase Plots for the "Best Case" Temperature Control: The five transformation regions are clearly visible. Note the movement of the transformation regions, most notably visible between $t = 0.6823$ ms and $t = 1.7548$ ms.

the Variable Viscosity Newton Method, Definition 4.1. We examine this through the following example, in which we use the same initial conditions and increased viscosities as required in the example 5.6. However, in this case we do not apply any external thermal control, and instead monitor the kinetic energy progression in time, given in Figure 5.18. We see that, indeed, the increased viscosity levels required at the onset of the martensitic phase transition affect the overall vibrational energy in the wire, but the resulting level of vibrational energy in the wire at the end of the simulation ($t = 2$ ms) are nearly 10 times larger than the vibrational energy levels resulting from the thermal damping case 5.6, as seen in Figure 5.14.

6 Conclusions on Current SMA and Active Damping

The results from Section 5.2 indicate that regularly-spaced transformation regions prove to be an integral tool in control schemes using the thermally-induced phase transition in shape memory alloys for vibration damping. However, in the computational experiments done here, the heat control implemented was much more powerful than anything currently practical. These excessive heating controls were used primarily because of the typically slow thermal response times associated with shape memory

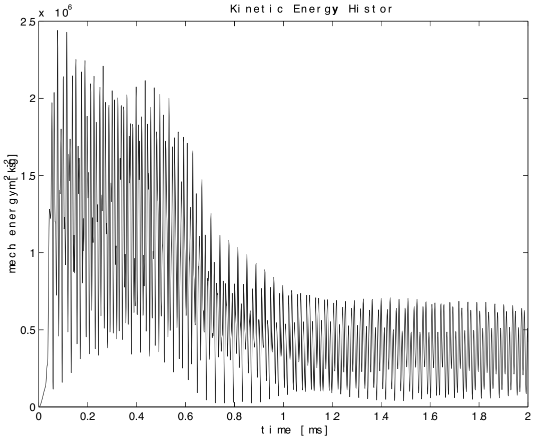

Fig. 5.18. Kinetic Energy Plot to Examine Viscous Effects: This example uses the increased viscosity levels resulting from the example 5.6, but without actively changing the temperature. Note the slight decrease in kinetic energy due to the viscous effects; however, significant levels of vibrational energy remain in the wire.

alloys, as evidenced by the large specific heat capacity c_p and small coefficient of thermal conductivity κ. Thus the excessive heating controls were used in order to shorten the simulation time required to observe phase transformations; however, the results pertaining to the onset of the phase transformation, as well as the suggested localization of the transformation regions, remains valid for even considerably less powerful thermal controls. Moreover, we predict that a possible "partially-active" control scheme corresponding to small, perpetually-transforming, slowly moving, distributed transformation regions along the wire will remain applicable for shape memory alloy damping devices. Theoretical aspects of this were studied by the authors in [24].

However, due to the slow response times associated with changes to the thermal field in shape memory alloys, truly active damping applications appear currently out of reach. Alternatively, other materials such as piezoelectrics and ferromagnetics, which undergo similar, though less-pronounced, phase transformations as a result of changes in the electric and magnetic fields, respectively, have significantly faster response times. This is because electrical and magnetic fields are more quickly changed than thermal fields. Therefore, the application of nonlinear models similar to the one proposed here, but applied toward those materials, may prove ideal for active vibration damping devices.

Another area for related work lies in the expansion of the current model to higher dimensions. We believe that the general nonlinear thermodynamic model from Section 2, and the overall solution method from Sections 3 and 4 would work similarly for the higher-dimensional case; however, the construction of applicable two-dimensional and three-dimensional forms of the Helmholtz free energy would prove much more complex. A starting point for such models would be the analysis of both the Falk-Konopka [11] and Ericksen-James [20–22] free energies. A further difficulty is that shape memory films and solids allow for the possibility of much more spatially complex temperature controls. However, it is our belief that a similarly-distributed "checkerboard" pattern of heating control for the thermally-activated damping would work well in such situations.

In our forthcoming work we look to the study of more complex vibrational excitations, such as single-frequency continued vibrational excitation at the free ($x = L$) end of the wire. In this work we hope to obtain thermal controls that will reduce the level of vibration as the continued excitations move through the transforming wire.

Our final item of note for the problem of thermally-activated actuation looks toward the development of future shape memory materials. Through changes in the consistency of particular elements, as well as material processes such as rolling and smelting, the thermal and mechanical properties of these alloys may be adjusted. Therefore, it may be possible to develop new shape memory materials with much faster thermal response times than current shape memory alloys allow. This may be possible through development of thinner wires and films, or by inclusion of materials having higher conductivity in the alloy mixture.

Moreover, considerable work is currently being done on heating and cooling devices to increase their strength, reduce their size and to improve their cycling frequency. To our knowledge, research in these areas is focusing on the development of cooling devices using the Peltier effect and heating devices based on the Joule effect. Advances in these areas may allow for increased controllability and localization in the thermal control of shape memory materials, therefore allowing for increased command over their phase transformations and behavior.

7 Appendix: Alternate Damping Possibilities

Our calculations show that the kinetic energy may be removed from a SMA wire by cancelling the oscillations of neighboring material points. Previous theoretical work on the use of SMAs for vibrational damping has also considered alternate mechanisms for this conversion between mechanical and thermal energy. The system can lose its energy also due to the motion of the Austenitic-Martensitic interface. We include a brief description of this phenomenon for the sake of completness.

R. Abeyaratne and J. Knowles have done a considerable amount of research on damping properties through their study of the interface dynamics between austenitic and martensitic regions in a transforming shape memory alloy [1,2]. Within these alloys, Abeyaratne and Knowles find that the movement of the austenite-martensite phase boundary acts as an active mechanism for conversion of mechanical to thermal energy (vibrations → heat). They consider the processes of shock- and stress-induced phase transformations in a purely mechanical model. Within this framework, they analyze processes using a combination of nonlinear elasticity and jump dynamics at the phase boundary.

To understand their analysis, we first consider the austenite-martensite phase boundary as a dynamic discontinuity, where the position of the interface is given by the function $s = s(t)$. Moreover, we define for any function $g = g(x,t)$ the jump function

$$\begin{aligned} [\![g(t)]\!] &= g^+(t) - g^-(t), \quad \text{where} \\ g^{\pm}(t) &= \lim_{x \to s(t)\pm} g(x,t); \end{aligned} \tag{7.1}$$

the value $[\![g(t)]\!]$ provides a measure of the discontinuity in g at the point $(s(t), t)$. Due to the regularity of the quantities of interest in the dynamic problem, the deformation u is continuous in x, while the deformation gradient γ is discontinuous across the phase discontinuity,

$$[\![u(t)]\!] = 0, \qquad [\![\gamma(t)]\!] \neq 0. \tag{7.2}$$

Combining the Clausius-Duhem inequality with the assumption that the entropy of a material element cannot decrease as it moves across strain discontinuity results in the relation [1,2]

$$f(t)\,\dot{s}(t) \geq 0. \tag{7.3}$$

Here, the function $f = f(t)$ denotes the driving force acting on the discontinuity at $s(t)$, given by

$$f(t) \;=\; \hat{f}(\gamma^-, \gamma^+) \;\overset{\text{def}}{=}\; \int_{\gamma^-}^{\gamma^+} \sigma(z)\,\mathrm{d}z \;-\; \frac{1}{2}\left(\sigma(\gamma^+) + \sigma(\gamma^-)\right)\left(\gamma^+ - \gamma^-\right) \tag{7.4}$$

We then define the *dissipation* $D(t)$ of mechanical energy on a small interval $(x_1, x_2) \subset (0, L)$ as the difference between the change in external work and the rate of change of total energy,

$$D(t) \overset{\text{def}}{=} (\sigma u_t)\big|_{x_1}^{x_2} - \frac{d}{dt}E(t), \tag{7.5}$$

where $E(t)$ denotes the total energy (kinetic + strain) in the interval (x_1, x_2) at time t. The field and jump equations then dictate that at points where γ, v are smooth,

$$\begin{aligned} \sigma'(\gamma)\gamma_x - \rho\, v_t &= 0, \\ v_x - \gamma_t &= 0; \end{aligned} \tag{7.6}$$

and at points where either γ or v jump across the curve $x = s(t)$, (7.6) becomes [1,2]

$$\begin{aligned} [\![\sigma]\!] + \rho\,\dot{s}\,[\![v]\!] &= 0, \\ [\![\gamma]\!]\,\dot{s} + [\![v]\!] &= 0. \end{aligned} \tag{7.7}$$

The equations (7.6) and (7.7), along with the definition (7.5) and the assumption (7.3), imply the following relation,

$$D(t) = f(t)\,\dot{s}(t) \geq 0. \tag{7.8}$$

Thus the dissipation may be thought of as the amount of work done *on* the bar *by* the moving discontinuity. As seen from (7.5), as D increases the total energy of the system decreases. Furthermore, since the driving force f is nonzero at the discontinuity $x = s(t)$ and the interface $s(t)$ is assumed to move, $f(t)\dot{s}(t) \neq 0$, and the overall energy of the system decreases proportionally to the speed of the phase boundary.

8 Acknowledgment

The authors are grateful to the anonymous referees for helpful suggestions and insightful comments that helped us to improve the quality of the presentation.

References

1. R. Abeyaratne and J. Knowles. On the driving traction acting on a surface of strain discontinuity in a continuum. *Journal of Applied Mechanics*, 38:345–360, 1990.
2. R. Abeyaratne and J. Knowles. Implications of viscosity and strain-gradient effects for the kinetics of propagating phase boundaries in solids. *SIAM J. Appl. Math.*, 51:1205–1221, 1991.
3. S.S. Antman. Physically unacceptable viscous stresses. *Z. Angew. Math. Phys.*, 49:980–988, 1998.
4. S.S. Antman and T.I. Seidman. Quasilinear hyperbolic-parabolic equations of one-dimensional viscoelasticity. *J. Diff. Eqns.*, 124:132–185, 1996.
5. S.S. Antman and T.I. Seidman. Parabolic-hyperbolic systems governing the spatial motion of nonlinearly viscoelastic rods. *(to appear)*, 2003.
6. M. Bokaie. Shape metal alloys. Technical report, TiNi Aerospace, Inc., San Leandro, CA, 2002. (www.tini-aerospace.com/sma.html).
7. C.M. Dafermos. *Hyperbolic Conservation Laws in Continuum Physics*, volume 325 of *Grundlehren der mathematischen Wissenschaften*. Springer-Verlag, Berlin Heidelberg, 2000.
8. A.F. Devonshire. Theory of ferroelectrics. *Adv. Phys.*, 3:86–130, 1954.
9. J.L. Ericksen. *Introduction to the Thermodynamics of Solids*. Applied Mathematics and Mathematical Computation. Chapman and Hall, London, 1991.
10. F. Falk. Landau theory and martensitic phase transitions. In L. Delaey and M. Chandrasekaran, editors, *International Conference on Martensitic Transformations*, pages 3–15. Les Editions de Physique, 1982.
11. F. Falk and P. Konopka. Three-dimensional Landau theory describing the martensitic phase transformation of shape-memory alloys. *Materials Science Forum*, 123-125:113–122, 1993.
12. D.A. French and S. Jensen. Long time behaviour of arbitrary order continuous time Galerkin schemes for some one-dimensional phase transition problems. *IMA Journal of Numerical Analysis*, 14:421–442, 1996.
13. D.A. French and T.E. Peterson. A continuous space-time finite element method for the wave equation. *Math. Comp.*, 65:491–506, 1996.
14. G. Friesecke and G. Dolzmann. Implicit time discretization and global existence for a quasi-linear evolution equation with nonconvex energy. *SIAM J. Math. Anal.*, 28(2):363–380, March 1997.
15. R.T. Glassey and J.W. Schaeffer. Convergence of a second order scheme for the semi-linear wave hyperbolic equations in 2 + 1 dimensions. *Math. Comp.*, 56:87–106, 1991.
16. K.-H. Hoffmann and Z. Songmu. Uniqueness for nonlinear coupled equations arising from alloy mechanism. Technical Report No 14, Center for Applied Mathematics, Purdue University, West Lafayette, 1986.
17. B.L. Hulme. One-step piecewise polynomial Galerkin methods for initial value problems. *Math. Comp.*, 26:415–426, 1972.
18. Y. Huo, I. Müller, and S. Seelecke. *Phase Transitions and Hysteresis*, chapter Quasiplasticity and Pseudoelasticity in Shape Memory Alloys, pages 87–146. Lecture Notes in Mathematics 1584. Springer-Verlag, Berlin, 1994. M. Brokate et. al., editors.
19. A.D. Johnson. Introduction to shape memory alloys. Technical report, TiNi Alloy Company, San Leandro, CA, 2001. (www.sma-mems.com/intro.html).
20. P. Klouček. Toward the computational modeling of nonequilibrium thermodynamics of the martensitic transformations. *IMA Preprint Series*, 1418, July 1996.
21. P. Klouček. The computational modeling of nonequilibrium thermodynamics of the martensitic transformations. *Computational Mechanics*, 22:239–254, 1998.
22. P. Klouček and M. Luskin. The computation of the dynamics of the martensitic transformation. *Continuum Mechanics and Thermodynamics*, 6:209–240, 1994.

23. P. Klouček and D.R. Reynolds. On the modeling of nonlinear thermodynamics in SMA wires. *Proc. R. Soc. Lond. A*, Submitted, May 2003.
24. P. Klouček, D.R. Reynolds, and T.I. Seidman. On thermodynamic active control of shape memory alloy wires. *Systems and Control Letters*, 48:211–219, 2003.
25. E.M. Lifshitz and L.P. Pitaevskii. *Statistical Physics by L.D. Landau and E.M. Lifshitz*, volume 5 of *Course of Theoretical Physics, Part I.* Pergamon Press, Oxford, 3rd edition, 1980.
26. V.A. Likhachev. Structure-analytical theory of martensite unelasticity. *J. de Physique*, IV:137–142, 1995.
27. J. Málek, J. Nečas, M. Rokyta, and M. Růžička. *Weak and Measure-valued Solutions to Evolutionary PDEs.* Applied Mathematics and Mathematical Computation 13. Chapman and Hall, London, 1996.
28. R.V.N. Melnik and A.J. Roberts. Approximate models of dynamic thermoviscoelasticity describing shape-memory-alloy phase transitions. In *New Methods in Applied and Computational Mathematics (NEMACOM'98).* Centre for Mathematics and its Applications, Nov. 1998.
29. R.V.N. Melnik and A.J. Roberts. Computational models for materials with shape memory: Towards a systematic description of coupled phenomena. In Sloot et al., editor, *ICCS 2002, LNCS 2330*, pages 490–499, Berlin, Heidelberg, 2002. Springer-Verlag.
30. I. Müller and S. Seelecke. Shape memory alloy actuators: Modeling and simulation. *ASME Applied Mechanics Reviews*, 56(6), 2003.
31. M. Niezgódka and J. Sprekels. Existence of solutions for a mathematical model of structural phase transitions in shape memory alloys. *Math. Meth. Appl. Sci.*, 10:197–223, 1988.
32. E.R. Oberaigner, T. Antretter, F.D. Fischer, and K. Tanaka. Optimized shape memory dampers, modelling and application. In *Proceedings of the Third World Conference on Structural Control 2002*, volume 2, pages 561–582. John Wiley & Sons, Ltd., 2003. F. Casciati, Edt.
33. R.L. Pego. Stabilization in a gradient system with a conservation law. *Proc. Amer. Math. Soc.*, 114, 1992.
34. D.R. Reynolds. *A Nonlinear Thermodynamic Model for Phase Transitions in Shape Memory Alloy Wires.* PhD thesis, Rice University, Houston, Texas, May 2003.
35. S. Seelecke. Modeling the dynamic behavior of shape memory alloys. *Int. J. Non-Lin. Mech., Special Issue on Hysteresis and its Implications in Mechanics*, 37:1363–1374, 2002.